Contents lists available at SciVerse ScienceDirect

Journal of Aerosol Science

journal homepage: www.elsevier.com/locate/jaerosci

Lagrangian/Eulerian model of coagulation and deposition of inhaled particles in the human lung

CrossMark

Lukas Pichelstorfer*, Renate Winkler-Heil, Werner Hofmann

Division of Physics and Biophysics, Department of Materials Research and Physics, University of Salzburg, Hellbrunner Strasse 34, 5020 Salzburg, Austria

ARTICLE INFO

ABSTRACT

The primary objectives of the present study were to mathematically describe particle coagulation within the human respiratory tract and to analyze its impact on local particle deposition patterns for high concentrations of inhaled cigarette smoke particles. Coagulation mechanisms simulated were thermal motion, gravitational settling, laminar shear, turbulences, electrical charges, and inertial effects at airway bifurcations. To implement concentration dependent coagulation processes, the Lagrangian random walk deposition model IDEAL, simulating the paths of an individual particle, was modified by tracking the random path of an elemental air volume containing the full size distribution, thus adding an Eulerian element to the Lagrangian random path model. In this combined Lagrangian/Eulerian deposition model, the initial size distribution is continuously modified by coagulation, hygroscopic growth and deposition. For the specific inhalation conditions and the cigarette smoke size distribution assumed in this study, thermal diffusion is by far the greatest source of coagulation, with a minor contribution of laminar shear in peripheral airway generations.

Number deposition, which comprises the loss of inhaled particles not only by deposition but also by coagulation, and mass deposition fractions were computed for different puff and breath-hold scenarios as a function of lung generation numbers. The main reduction of the number of inhaled particles in the respiratory tract occurs in the mouth due to coagulation, accompanied by a significant shift of the size distribution to larger particle diameters. In the lung, particle loss is caused primarily by deposition due to diffusion with a preferential deposition of smaller particle diameters. In the size range from about 250 to 500 nm, the number concentration of particles in the exhaled air is higher than that in the inhaled air, indicating that the production of particles in this size range by coagulation is greater than the loss by coagulation to larger sizes and deposition.

1. Introduction

A key parameter for the simulation of the deposition of aerosol particles in the human respiratory tract is their diameter. There are two mechanisms that can cause a change in particle diameter. The first mechanism is phase transitions of volatile substances in the system, such as hygroscopic growth. There are several papers addressing this topic (Ferron et al., 1988; Robinson & Yu, 1998; Longest & Kleinstreuer, 2005). The second mechanism, which is the focus of this article, is coagulation of aerosol particles at high concentrations.

* Corresponding author. Tel.: +43 662 8044 5718; fax: +43 662 8044 150.
  E-mail address: Lukas.Pichelstorfer@sbg.ac.at (L. Pichelstorfer).

Nomenclature

A	cross section area	β	coagulation coefficient
Cc	Cunningham correction factor	Δ	difference
d	particle diameter	ε_d	energy dissipation by turbulence
d_{jet}	jet diameter	Θ	half of the branching angle at a bifurcation
D	diffusion coefficient	η	viscosity
E	empirical capture efficiency for two particles	ρ	density
E_I	deposition efficiency	Φ	correction factor for thermal coagulation
g	acceleration of gravity		
n_i	number concentration of particles in size bin i	*Subscripts*	
r	radial distance, $r = \sqrt{x^2 + y^2 + z^2}$		
S	stopping distance	i, j, k	particle of size bin i, j, k
Stk	Stokes number	gen	lung generation
t	time	grav	gravitation
U	particle velocity	p	particle
v_{gas}	gas velocity	sv	settling velocity
x	removed particle fraction due to coagulation	therm	thermal
		trans	transition regime

There are various types of coagulation mechanisms, which can be characterized by their source of relative motion causing inter-particle collisions. Previous studies on particle deposition in the lung (Robinson & Yu, 1999; Ingebrethsen et al., 2011; Mitsakou et al., 2004) focused on thermal coagulation, where particles collide and adhere to each other due to their thermal motion. Other mechanisms leading to particle coagulation are gravitational settling, laminar shear or turbulent flows, and inertial effects at bifurcations. These mechanisms are currently not included into any model describing particle deposition in the human respiratory system. Furthermore, the charging state of the aerosol can have an impact on the coagulation rate (Fuchs, 1964). While thermal motion and gravitational settling are active throughout all regions of the human respiratory system, laminar shear requires a laminar whereas coagulation due to turbulences requires a turbulent flow field. It has been demonstrated that turbulences occur primarily in the extrathoracic (ET) region, while the flow field becomes more and more laminar with increasing penetration into the lung (Martonen, 1993). The transition from turbulent to laminar flow also depends on the breathing pattern. The deviation of particles from the streamlines at bronchial airway bifurcation represents another effect leading to coagulation.

Since coagulation of aerosol particles is solely effective for high particle concentrations we applied cigarette smoke inhalation to demonstrate the effect of coagulation on particle deposition. There are numerous publications about cigarette smoke size distributions published in different research areas, such as tobacco science, aerosol science or respiratory toxicology. As stated by Alderman & Ingebrethsen (2011), the results differ widely due to the high dynamics of the fresh combustion aerosol. The reported average diameters on a count basis vary from 160 to 600 nm. However, recent measurements featuring well defined mixing ratios of clean air and cigarette smoke and aging times show better agreement (Adam et al., 2009; Alderman & Ingebrethsen, 2011; Kane et al., 2010).

To roughly characterize aerosol deposition modeling one may distinguish between empirical and mechanistic models. Empirical models are easy to use, but they are restricted to the conditions they are derived from. A review on empirical lung deposition models is given in ICRP (1994). Mechanistic models are somewhat more diverse. They apply either deterministic or stochastic (e.g. Monte Carlo) methods to describe the aerosol flow in the human respiratory tract (HRT). Furthermore, simulations may be Eulerian or Lagrangian. The former focuses on the population of the particles that are tracked through the HRT while the later follows trajectories of single particles. Some models apply computational fluid dynamics (CFD) methods to accurately account for the morphology and resulting flow patterns, while others are based on idealized descriptions. Detailed descriptions of mechanistic aerosol deposition models are given by Finlay (2001) and Hofmann (2011). The present model is mechanistic in nature, applying Monte Carlo simulations and Lagrangian as well as Eulerian methods.

The primary objectives of the present study are (i) to mathematically describe particle coagulation within the human respiratory system, and (ii) to analyze its impact on local particle deposition patterns of inhaled cigarette smoke particles.

2. Material and methods

2.1. Coagulation model

To describe the impact of coagulation on the particle size distribution the following equation has been applied (Smoluchowski, 1917):

$$\frac{dn_k}{dt} = -\sum_{i=1}^{s} \beta_{ik}(\cdots)n_i n_k + \frac{1}{2}\sum_{f(i+j)=f(k)} \beta_{ij}(\cdots)n_i n_j \tag{1}$$

where n_i is the concentration of particles i, t is the time and s is the number of different particle sizes, β_{ik} is the coagulation coefficient of colliding particles i and k which varies its form according to the coagulation mechanism observed. While Smoluchowski applied this formula solely to describe thermal coagulation, it forms the basis for the description of various coagulation mechanisms in the present study.

The following mechanisms causing coagulation were investigated:

- Thermal motion;
- Gravitational settling;
- Laminar shear;
- Turbulences;
- Electrical charges;
- Inertial effects at airway bifurcations.

Note that the probability of adhering to each other after a collision (i.e. the accommodation coefficient) was assumed to be equal to 1 for all of the models listed.

Airborne particles move randomly in a gas atmosphere due to thermal forces, resulting in statistical collisions. These collisions are limited depending on the ratio of the particle's mean free path to the particle diameter, the so-called Knudsen number (Kn) (Truesdell & Muncaster, 1980). In case of small Kn (i.e. the continuum regime), coagulation is limited by diffusion, and for high Kn (i.e. the kinetic regime), gas kinetics govern the process and the particles' cross sections are the limiting factor. The cigarette smoke size distribution modeled in this study is situated in the transition region between the two regimes. Accurate description of the transition regime is very complex. Therefore, an approximation for the coagulation coefficient was employed, derived from Fuchs (1964):

$$\beta_{therm,trans,ik} = \pi(d_i + d_k)(D_i + D_k)\Phi_{trans,ik} \tag{2}$$

where d_i and D_i are the diameter and diffusion coefficient of particle i, respectively, $\Phi_{trans,ik}$ is the function accounting for the transition from the continuum to the kinetic regime for decreasing particle diameters.

The charging state of the particles also influences the frequency of thermal particle collisions. To account for this we applied the following coagulation coefficient derived from Fuchs (1964)

$$\beta_{therm,charge,ik} = \beta_{therm,ik}\Phi_{charge,ik} \tag{3}$$

where $\beta_{therm,ik}$ is the coagulation coefficient describing thermal induced collisions of neutral particles in the continuum regime, $\Phi_{charge,ik}$ is the correction factor that accounts for the altered collision probability due to the influence of charge.

Though they may remain in the ambient air for a considerable amount of time, airborne particles settle due to gravitational forces. Some particles settle faster, others slower, depending on their aerodynamic diameter. The difference in their settling velocities is another source of coagulation. A coagulation coefficient for gravitational settling was derived from Hinds (1999):

$$\beta_{grav,ik} = \pi\left(\frac{d_i + d_k}{2}\right)^2 \Delta U_{sv,ik}E_{ik} \tag{4}$$

where $\Delta U_{sv,ik}$ is the relative velocity of particle i and k, and E_{ik} is the empirical efficiency for particle i being captured by particle k.

Furthermore, coagulation depends on the flow pattern. For laminar flows the particle velocity is a parabolic function of the distance from the centerline of the given airway generation. Particles traveling on neighboring streamlines may collide due to their relative motion. The coagulation coefficient for laminar flows was derived from Zebel (1966):

$$\beta_{shear,ik} = \frac{16\pi}{3}\left(\frac{d_i + d_k}{2}\right)^3 \frac{U_{gen,j}}{A_{gen,j}} \tag{5}$$

where $U_{gen,j}$ and $A_{gen,j}$ are the mean airflow velocity and the cross section of generation j, respectively.

An approximate expression for coagulation due to turbulences in the airways is given by given by Saffmann & Turner (1956):

$$\beta_{turb,ik} = 1.3\left(\frac{d_i + d_k}{2}\right)^3 \left(\frac{\epsilon_d\rho_{gas}}{\eta}\right)^{\frac{1}{2}} \tag{6}$$

where ρ_{gas} is the gas density, η is the gas viscosity and ϵ_d is the energy dissipation by turbulence.

At a bronchial airway bifurcation with branching angle Θ, particles may leave the streamlines due to inertia and travel with relative speed compared to the new direction of the gas flow. These differences in particle inertia can also cause coagulation:

$$\beta_{bif,ik} = \pi\left(\frac{d_i + d_k}{2}\right)^2 v_{gas}\sin(\Theta)E_{ik} \tag{7}$$

where d_i is the particle diameter of particle i, v_{gas} is the gas speed and E_{ik} the empirical efficiency for particle i being captured by particle k.

The time for coagulation is then given by:

$$\Delta t = \frac{1}{v_{gas} \sin(\Theta)} |S_i - S_k| \tag{8}$$

where S_i is the stopping distance of particle i (Hinds, 1999). The derivations of Eqs. (7) and (8) are explained in more detail in Appendix A.

An estimate whether coagulation will play a role or not can be derived from Hinds (1999), where the number concentration of particles $n(t)$ is given as a function of the initial particle number concentration n_0, coagulation coefficient β and coagulation time t for monodisperse particle size distributions:

$$n(t) = \frac{n_0}{1 + n_0 \beta t} \tag{9}$$

The removed particle fraction due to coagulation x is then given by

$$x = 1 - \frac{n(t)}{n_0} = \left[\frac{1}{n_0 t \beta} + 1\right]^{-1} \tag{10}$$

which can be approximated by $x \cong n_0 t \beta$ for small changes of number concentrations. Although this equation describes an idealized situation, the expression for x can be used to estimate whether coagulation can be neglected. Note that the expression derived is valid only for monodisperse or very narrow particle size distributions. Hence this method is not applicable to settling coagulation and coagulation at lung bifurcations which are caused by differences in particle settling velocities and inertial forces, respectively.

The computational coagulation model was programmed using Visual Fortran (version 6.6). The structure of the code is basically the same for every type of coagulation, i.e. particles collide due to their relative motion and thus form a bigger particle. For practical reasons, the size distribution considered is discretized in terms of size bins. The current model features 90 size bins in which particles are classified before the coagulation process starts. Each size bin has a width of 5% of its mean diameter. The variable governing the whole coagulation process is time. The total coagulation time t_{tot} is divided into time steps t_{step}. For one time step the interaction of all size bins is computed and the various coagulation mechanisms are simulated in a consecutive manner.

Since the mass is preserved, particles are solely formed by coagulation of other particles. The size distribution is represented by a number of size bins, each characterized by its mean diameter and width, and hence some information about the mass in the system is lost when particles move to another size bin. The arising uncertainty in mass is recorded by the program (it was below 1% for all simulations). The result of the simulation is the evolution of the initial size distribution. From this raw data, various types of information like average particle diameter, average particle mass, particle number concentration, and particle charge distributions are calculated for a series of time steps during inhalation and exhalation.

2.2. Implementation of the coagulation model into a stochastic deposition model

The human respiratory tract is commonly divided into three major regions depending on anatomical and physiological differences (ICRP, 1994): (1) the extrathoracic (ET) region, extending from the nose or the mouth to the entrance of the trachea, acting as a protective filter for the lung, (2) the tracheobronchial region of the lung, composed of bronchial (BB) and bronchiolar (bb) airways and ranging from the trachea to the terminal bronchioles, where inhaled air and entrained particles are conducted to the peripheral parts of the lung, and (3) the alveolar-interstitial (AI) or acinar region, where the gas exchange between inhaled air and blood takes place via the alveoli. For a detailed graphical and numerical description of the anatomical features and physiological functions of these regions the reader is referred to the ICRP (1994) report.

Morphometric lung models always refer to the lung (or thoracic region), consisting of BB, bb and AI regions. Different morphometric models have been published in the past, characterizing the branching network of bifurcating bronchial and acinar airways at different levels of sophistication (Hofmann, 2011). The asymmetric stochastic airway geometry of the human lung employed in this study is based on rigorous statistical analyses of the morphometric data of bronchial (Raabe et al., 1976) and acinar (Haefeli-Bleuer & Weibel, 1988) airways (Koblinger & Hofmann, 1985). For the deposition calculations, the measured morphometric data were scaled down to a functional residual capacity (FRC) of 3300 cm³ (ICRP, 1994) and an oropharyngeal region of 50 cm³ was attached to the trachea.

The stochastic, asymmetric deposition model IDEAL allows the calculation of total, regional, lobar and generational deposition fractions for defined particle diameters and breathing conditions. In this Lagrangian deposition model, which was originally developed by Koblinger & Hofmann (1990), and Hofmann & Koblinger (1990) and further extended by Hofmann et al. (2002, 2008), the trajectories of single particles through a stochastic airway geometry are simulated by Monte Carlo methods. The smallest geometric airway unit for which deposition fractions are calculated are Y-shaped bifurcations, consisting of half of the parent plus half of the successive daughter airway.

For the simulation of random paths through the lungs, the geometric properties of the two daughter airways are randomly selected at each bifurcation from their probability density functions, although constrained by correlations among

some of the parameters. The actual path of the particle through either the major or the minor daughter branch is randomly selected from the flow splitting distribution based on distal lung volumes. Upon expiration, particles follow the same path as during inspiration. However, due to partial mixing with the residual air in alveoli, particles may not follow the first-in/ last-out approximation. By simulating the random paths of many particles, typically of the order of tens or hundreds of thousands, statistical means can be calculated for total, regional, and generational deposition, providing also information on the underlying statistical distributions.

Since information on transport and deposition of individual particles within airway bifurcations is limited at present to only a few selected bifurcation models (Balásházy et al., 2003; Farkas et al., 2006; Zhang et al., 2009), deposition in individual airways is currently based on the average behavior of an ensemble of particles as given by analytical equations for different deposition mechanisms.

Deposition by Brownian motion in upper bronchial airways was determined by the empirical equation proposed by Cohen and Asgharian (1990) to account for enhanced deposition due to developing flow. In more peripheral bronchiolar and acinar airways, Ingham's (1975) equation for diffusion under parabolic flow conditions was applied, while for expiratory flow a uniform flow profile due to secondary flows was assumed for all airways (Ingham, 1975). Deposition by inertial impaction in bronchial airways was calculated according to Cai & Yu (1988), assuming a uniform profile in upper bronchial airways, a parabolic profile in distal bronchiolar and acinar airways, and again a uniform profile upon expiration. In the trachea, the effect of the laryngeal jet was considered by the empirical equation proposed by Chan et al. (1980). Finally, deposition by sedimentation was computed by the equations proposed by Finlay (2001) for well-mixed plug flow in upper bronchial airways, Poiseuille flow in bronchiolar airways, laminar plug flow in alveolated airways, and well-mixed plug flow in all conducting airways during exhalation. Because of the geometric complexity of the oropharyngeal region, its filtering efficiency was considered by the semi-empirical equations derived by Cheng (2003) for the diffusion regime and by Stahlhofen et al. (1989) for the impaction regime for both inspiration and expiration.

This stochastic deposition model was validated by comparison with the experimental data of Heyder et al. (1986) for small and large particles and of Schiller et al. (1988) for ultrafine particles, and the fitted deposition data provided by the ICRP (1994) for both total and regional deposition (Hofmann, 2011). Thus the excellent agreement with these experimental data for individual particles, where coagulation can safely be neglected, provides a reliable basis for the simulation of deposition patterns of highly concentrated particles. In the present case of cigarette smoke inhalation after the breath-hold period in the mouth, particle transport into the lungs is characterized by an aerosol bolus with a width of 50 cm³, representing the volume of the oral cavity (Hofmann et al., 2008).

In the original deposition model, the diameter of a particle is randomly selected from a defined size distribution and the random path of this particle through the random airway system is tracked during a full breathing cycle until it is either deposited or exhaled. In case of hygroscopic particles, the diameter of the particle is modified in each airway bifurcation according to the specific growth factor in that generation (Ferron et al., 1988). In case of inhalation of aerosols with high particle concentrations, however, the diameter of a particle also increases due to coagulation as a function of the aerosol concentration in a given airway bifurcation, i.e. the initial size distribution prior to the onset of inhalation is no longer constant. Thus to calculate the correct diameter in a given airway bifurcation requires information on the particle concentration in that specific bifurcation, which continuously decreases as particles penetrate deeper into the lungs. In addition to particle losses due to coagulation, particle concentrations are also reduced by the various deposition processes.

To implement the concentration dependent coagulation processes into the stochastic deposition model IDEAL, it was necessary to modify the currently existing code. Instead of tracking an individual particle, the random path of an elemental air volume containing the full size distribution was simulated, thus adding an Eulerian element to the Lagrangian random path model. In this combined Lagrangian/Eulerian deposition model, the initial size distribution is continuously modified by coagulation, hygroscopic growth and deposition. Because of the Lagrangian nature of the deposition model, these simultaneously occurring processes are treated independently in a consecutive fashion. To minimize the effect of considering these mechanisms consecutively rather than simultaneously, airway bifurcations were divided into a series of tubular segments or time intervals. At present, the length of a given individual time interval is determined by a maximum change of the concentration by 1% in all diameter intervals. Deposition probabilities are then calculated for each airway segment by segment until the size distribution has exited the whole airway bifurcation, entering the next bifurcation downstream.

2.3. Deposition in the oral region during puffing and breath-hold

Particle deposition in the oral region during puffing and breath-hold was computed for diffusion, inertial impaction and gravitational settling, with diffusion being the dominant deposition mode.

To assess the reduction in particle concentration due to diffusion, radial diffusion in a sphere was considered based on the root mean square displacement of a particle (Einstein, 1905):

$$r = \sqrt{6Dt} \tag{11}$$

with $r = x^2 + y^2 + z^2$, where x, y, and z form a Cartesian coordinate system. D is the diffusion coefficient of the particle and t is the time.

Impaction of particles occurs on the back wall of the oral cavity. Cigarette smoke enters the mouth with a given velocity which is determined by the volume flow and the cigarette diameter. Deposition efficiency E_I was derived from Hinds (1999):

$$E_I = \frac{\pi}{2} Stk \tag{12}$$

where the Stokes number Stk is given by

$$Stk = \frac{\rho_p d^2 U Cc}{9 \eta d_{jet}} \tag{13}$$

where U is the particle velocity, and d_{jet} is the jet diameter which is assumed to be the diameter of the cigarette filter.

Particle loss due to gravitational settling was calculated for a cuboid having the same volume as the mouth cavity. The particle settling velocity given by Hinds (1999) was applied:

$$V_S = \frac{\rho_p d^2 g Cc}{18 \eta} \tag{14}$$

where ρ_p is the particle density, d is the particle diameter, g is the acceleration of gravity, Cc is the Cunningham correction factor and η is the gas viscosity.

3. Results

3.1. Coagulation

The model has been used to calculate coagulation due to the mechanisms described in Section 2.1 during inhalation of a highly concentrated cigarette smoke aerosol. The initial particle size distribution has been taken from Ingebrethsen et al. (2011), assuming a lognormal distribution with an average particle diameter of 0.15 μm, a geometric standard deviation of 1.44, and a total concentration of 1.54×10^9 particles per cm^3. It is further assumed that cigarette smoke particles are spherical liquid particles, thus forming again spherical particles after coagulation.

Figure 1 depicts the coagulation coefficients for five different sources of coagulation as a function of particle diameter ratio, where the numerator was varied from 1 nm to 100 μm, while the denominator was kept constant at 100 nm. The values were calculated for the reference respiratory parameters characteristic of a male person under sitting breathing conditions as defined in ICRP Publication 66 (ICRP, 1994) with a tidal volume of 750 mL and a breathing frequency of 12 breaths per minute, resulting in a flow rate of 300 cm^3 s^{-1}. Thermal as well as gravitational settling coagulation exhibit a minimum for particles of equal size. For comparison, laminar shear coefficients calculated for airway generation 15 and turbulent coagulation coefficients calculated for airway generation 3, rise monotonically with increasing particle size. Coagulation at bifurcations due to differences in particle inertia was calculated for the bifurcation of the main bronchus. Though coagulation at bifurcations features a considerable coagulation coefficient, its contribution to total coagulation is
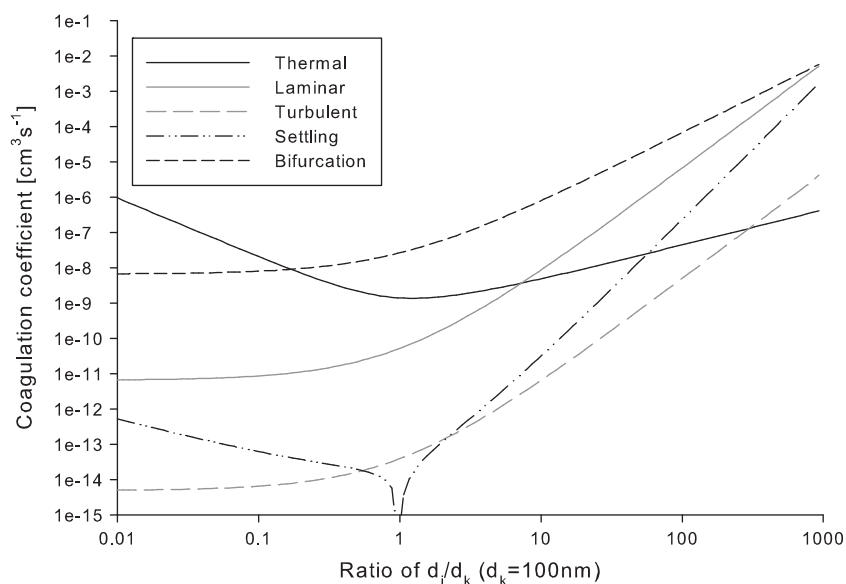
Fig. 1. Coagulation coefficient as a function of the diameter ratio of colliding particles. The coagulation coefficient for laminar flow and turbulent flow were calculated for airway generations 3 and 15, respectively.

practically negligible since the time for coagulation is small (see Eq. (8) and Fig. 4) compared to the other mechanisms. Therefore, Fig. 1 clearly demonstrates the dominance of thermal coagulation for particles in the size range or smaller than 100 nm at the assumed flow pattern. However, corresponding calculations for larger particles revealed that laminar shear coagulation may exceed thermal coagulation for particle sizes greater than about 400 nm.

The effect of the charging state on coagulation was simulated using the charge distribution suggested by Robinson & Yu (1999). Based on experimental data they assumed a symmetric charge distribution, where 45% of the particles were neutral, 47% carried one elementary charge and 8% carried two elementary charges. To assess the contribution of the charging state of particles on the coagulation rate, the ratio of the thermal coagulation coefficient of charged particles to the neutral thermal coagulation coefficient is illustrated in Fig. 2. There, the average ratio of the attracting and the repelling term for symmetrically bipolar charged, monodisperse aerosols is plotted against particle diameter. The thermal coagulation coefficient was derived using Eq. (2) without the correction factor for the transition regime and the thermal coagulation coefficient for charged particles was calculated by arithmetically averaging the coagulation coefficients for the repelling (i.e. collision of like charged particles) and the attracting (i.e. collision of unlike charged particles) cases using Eq. (3).

For colliding particles with an initial average particle diameter of 150 nm and a GSD of 1.44, the simulation revealed little influence of the charge on the coagulation process and predicts a ratio of charged coagulation to uncharged coagulation close to one. The reason for this behavior can be found in the evolution of the charge distribution, which remains fairly constant during the whole coagulation process. Although elementary charge numbers of 5 and more per particle may occur within fractions of a second, their number concentration is too low to significantly influence the collision process. Therefore, coagulation for an average particle size of 150 nm is mainly driven by collision of neutral and singly charged particles, where the latter can safely be approximated by the behavior of uncharged particles.

For example, the distributions of the coagulation coefficients for a 260 nm particle colliding with a 440 nm particle among human airway generations are displayed in Fig. 3. Particle sizes of 260–440 nm are representative for the aged aerosol size distribution in the lungs following coagulation in the mouth and hygroscopic growth in upper bronchial airways, originating from an inhaled fresh aerosol in the size range from 100 to 300 nm. Figure 3 also depicts the mean residence times within the human lung generations. For these calculations, the temperature within the lung was kept constant. As a result, coagulation coefficients that do not depend on the flow pattern are constant throughout the whole lung. Note that coagulation due to turbulences disappears and turns to laminar shear coagulation as the flow gets laminar in peripheral airways. Similar to Fig. 1, coagulation at bifurcations features a high coagulation coefficient although its contribution to total coagulation is small due to very limited coagulation time (see Fig. 4). Except between airway generations 12 and 19, where laminar shear flow is the main contributor to coagulation for the observed particle diameters, thermal coagulation dominates in the remaining airways. Note that flow dependent coagulation was not computed for the oral region.

The coagulation coefficient for particle collisions caused by their different inertia and the time available for coagulation as a function of the diameter ratio of the colliding particles are plotted in Fig. 4. Here the numerator was varied from 1 nm to 100 μm, while the denominator was kept constant at 100 nm. This calculation refers to the first airway bifurcation, where the trachea branches into the two main bronchi. Compared to the coagulation times for the other mechanisms described
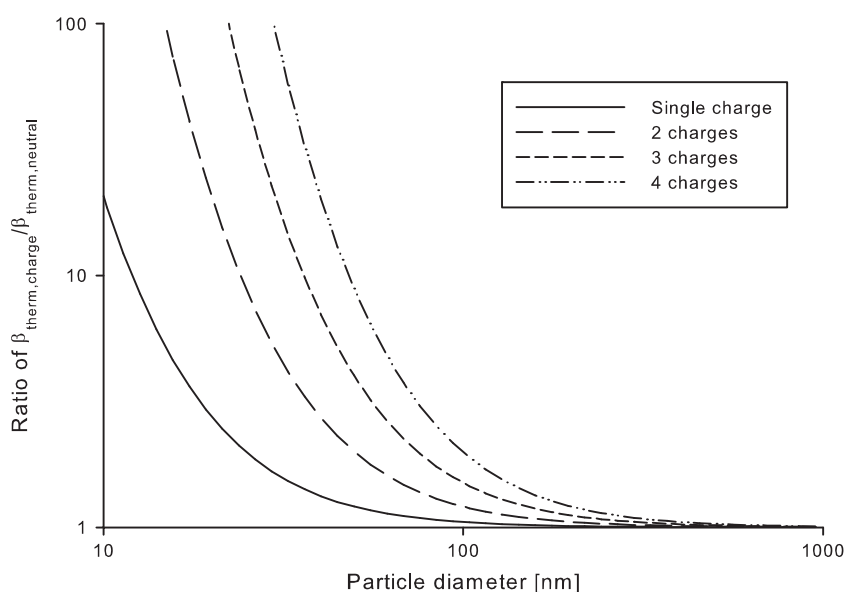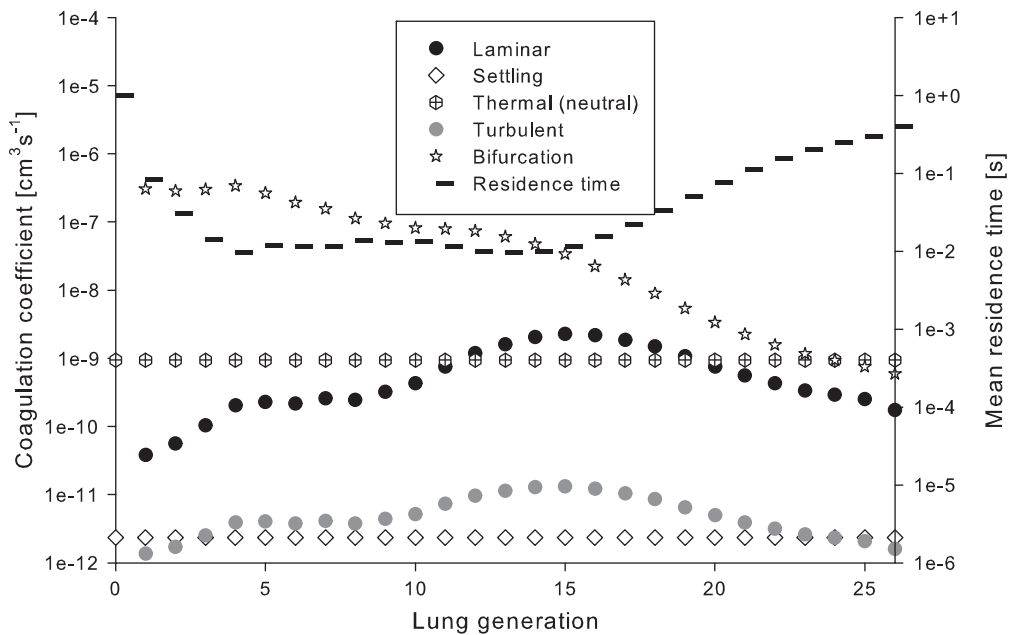

Fig. 2. Ratio of monodisperse charged to monodisperse uncharged coagulation coefficients as a function of particle diameter for different symmetric bipolar particle charging states.

Fig. 3. Coagulation coefficient for particle diameters of 260 nm and 440 nm (left-hand side ordinate), and mean residence time (right-hand side ordinate) as a function of lung generation.
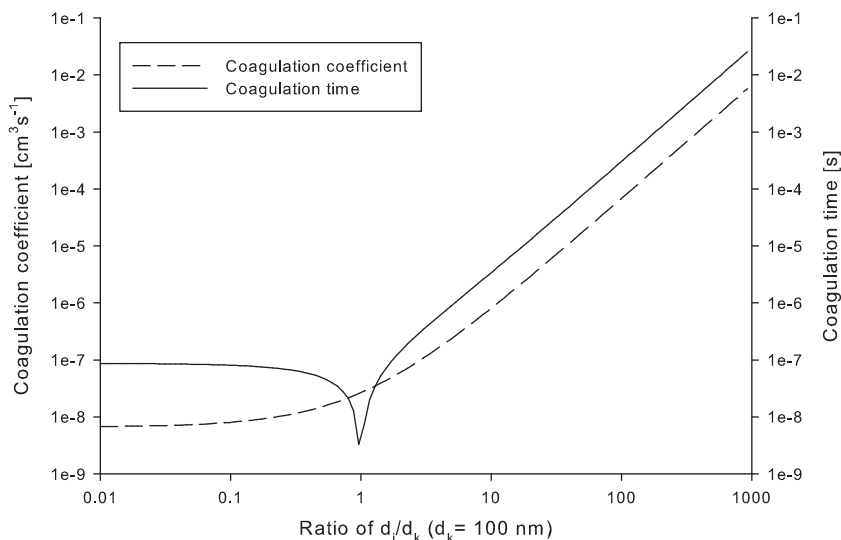
Fig. 4. Coagulation coefficient and coagulation time caused by the differences in particles' inertia at the trachea—main bronchi bifurcation, both as a function of the diameter ratio of the colliding particles.

(thermal, laminar shear, turbulent and settling coagulation), which are of the order of seconds, coagulation time for coagulation at bifurcations is below 10^{-7} s for a fresh cigarette smoke size distribution as given by Ingebrethsen et al. (2011).

The impact of the smoking behavior on the resulting size distribution and, in further consequence, on deposition is illustrated in Fig. 5. Here, the average particle diameter is plotted as a function of the puffing time during which the cigarette smoke is introduced into the mouth cavity. The topmost curve simply represents aging of the aerosol. The increase in average particle diameter with time is practically entirely caused by thermal coagulation as the coagulation coefficients of the other mechanisms are orders of magnitude smaller. The lowest curve shows the aging of the aerosol when fresh particles are permanently added at a rate of 25 ml s^{-1} during the puffing time.

The evolution of the size distribution during the aerosol's residence in the mouth was calculated for a puff time of 2 s and a subsequent breath-hold time of 1 s, which has been found to represent the commonly observed smoking scenario (Ingebrethsen et al., 2011). The initial size distribution, the size distribution immediately after the puff and after
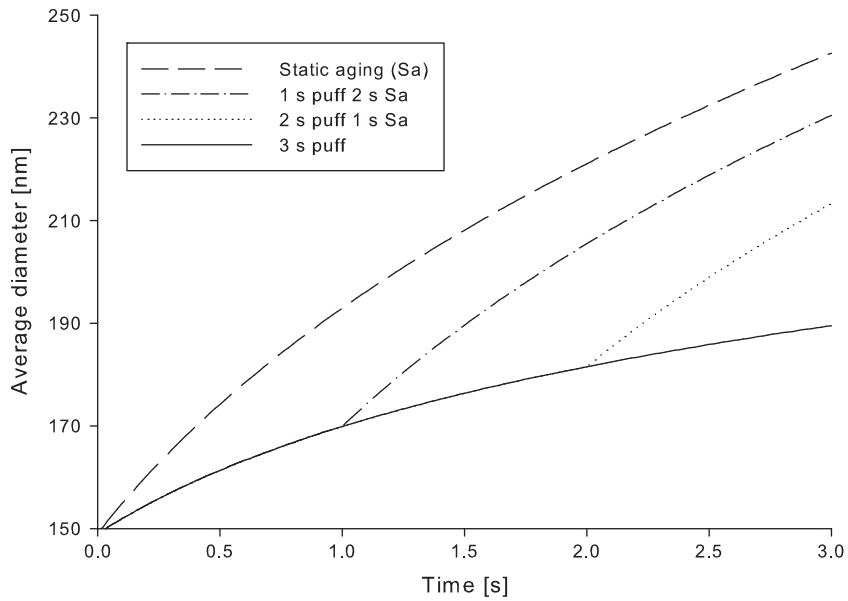
Fig. 5. Evolution of the average particle diameter for various puffing durations and breath hold times as a function of time.
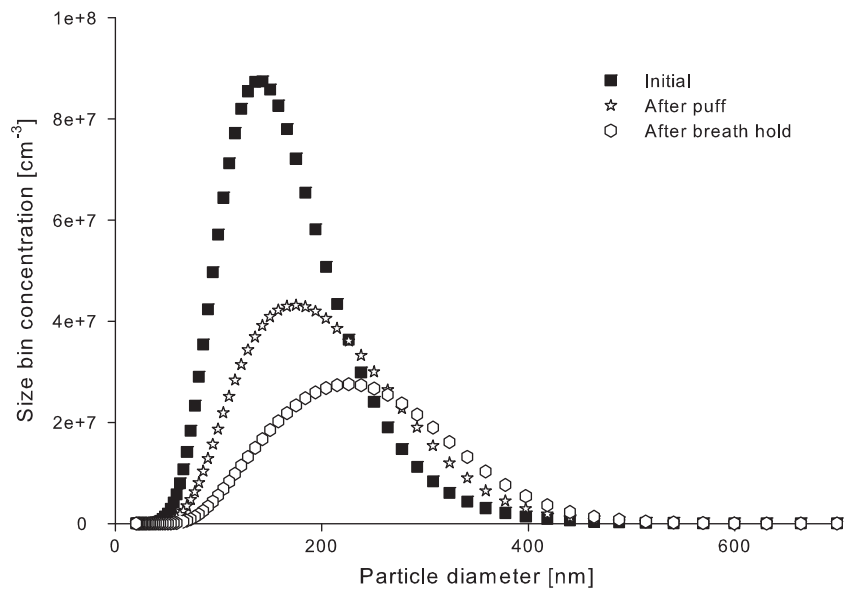

Fig. 6. Particle number concentrations in the predefined size-bins for three different points in time: (i) Initial particle size distribution, (ii) particle size distribution at the end of the 2 s puff, and (iii) particle size distribution 1 s after the end of the puff.

the breath-hold, respectively, are plotted in Fig. 6, indicating rapid changes in total concentration and related shift of the shape of the size distribution to larger diameters. The number of particles below about 100 nm decreases to almost zero. Also, the number of particles between 100 nm to about 230 nm decrease, whereas particles larger than about 250 nm are newly formed by coagulation.

In summary, we find quite significant changes in particle number and size distributions due to coagulation while the aerosol is still kept in the oral cavity.

The effect of variations in breath-hold times on the resulting size distribution in the oral cavity is depicted in Fig. 7 for a constant puff time of 2 s and an inhalation time of 0.167 s (*note*: the inhalation time is defined as the time it takes the puff to exit the mouth for the assumed flow rate). The size distributions plotted in this figure represent the exit distributions from the oral cavity and hence the input distributions into the human airway system. With increasing breath-hold time and
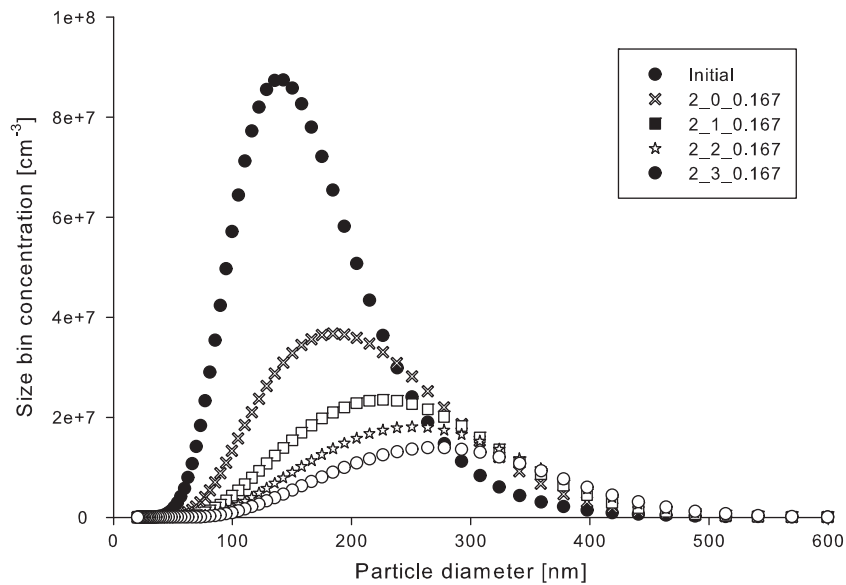
Fig. 7. Effect of breath-hold time variations on the number size distribution at the beginning of inhalation into the lung for a puff time of 2 s and an inhalation time of 0.167 s.
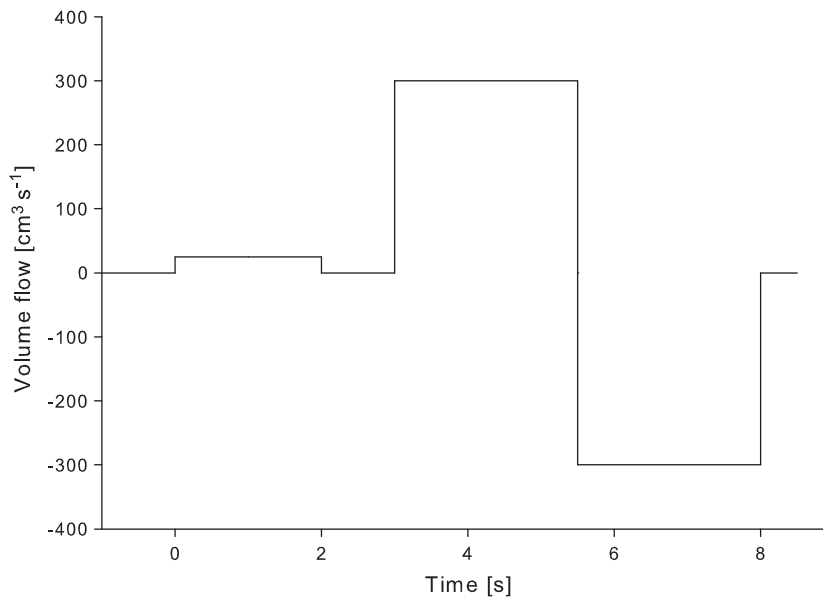

Fig. 8. Breathing/puffing waveform adapted to smoking: Volume flow in cm^3 as a function of time in s for puffing (0-2 s), breath-hold (BH, 2-3 s), inhalation (3-5.5 s) and exhalation (5.5-8 s).

hence more time available for coagulation, and extrathoracic deposition, the size distributions are continuously shifted to higher diameters, accompanied by an ever increasing loss of particles. A very similar pattern can be observed in for variations in puffing time and constant breath-hold time. Here, a longer puff time allows again more time for the coagulation processes, resulting in rising particle diameters and decreasing particle concentrations.

3.2. Transport and deposition

Differential number deposition of inhaled 150 nm CMD particles (GSD=1.44) with a particle concentration of 1.54×10^9 particles per cm^3 and a flow rate of 300 cm^3 s^{-1} (tidal volume=750 cm^3 and inhalation time=2.5 s; puffing breathing waveform depicted by Fig. 8) are plotted in Fig. 9 as a function of lung generation numbers for different puff and breath-hold scenarios. Breathing scenarios comprise normal bolus breathing (0_0) to bolus inhalation with a puff time of 2 s and varying breath-hold times ranging from 0 s (2_0) to 1 s (2_1) and 2 s (2_2), where the standard smoking scenario is defined by a puff
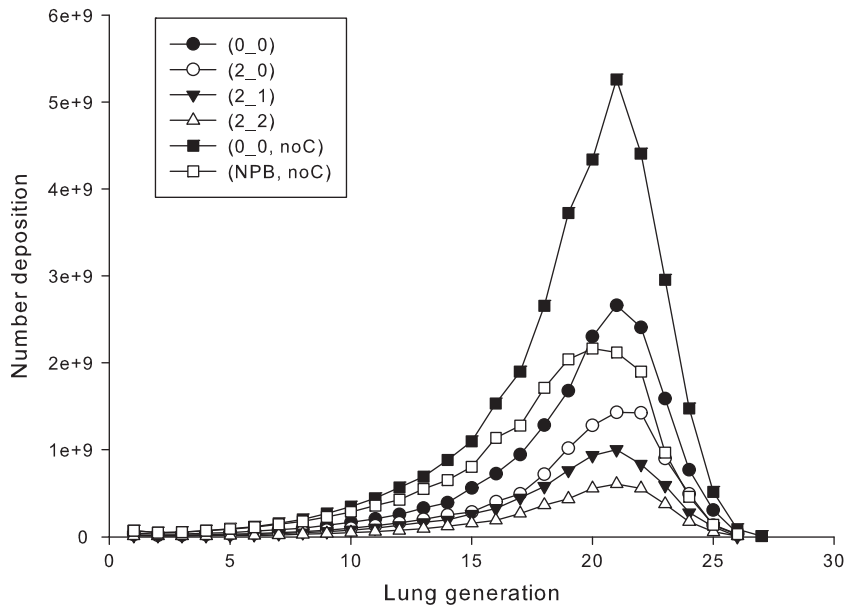
Fig. 9. Number deposition of inhaled 150 nm CMD particles (GSD=1.44) (inhaled particle concentration=1.54 × 10⁹ particles per cm³) as a function of lung generation numbers for a flow rate of 300 cm³ s⁻¹ (tidal volume=750 cm³ and inhalation time=2.5 s) and different puff and breath-hold scenarios: (0_0) normal bolus breathing (0_0), puff time=2 s, no breath-hold (2_0), puff time=2 s, breath-hold time=1 s (2_1), and puff time=2 s, breath-hold time=2 s (2_2). For comparison, number deposition without considering coagulation for normal bolus inhalation (0_0, noC) and for normal physiological breathing (NPB, noC) are also plotted.
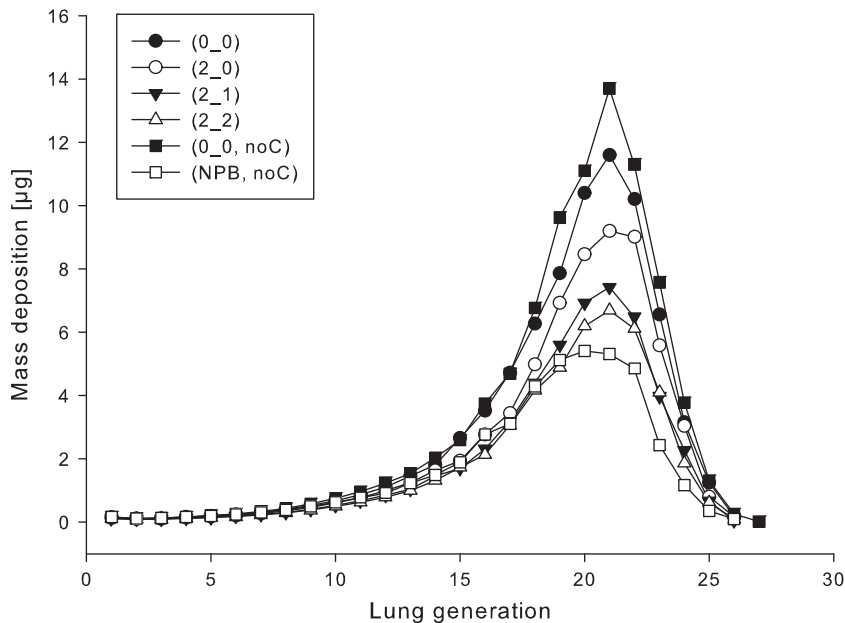
Fig. 10. Mass deposition of inhaled 150 nm CMD particles (GSD=1.44) (inhaled particle concentration=1.54 × 10⁹ particles per cm³) as a function of lung generation numbers for a flow rate of 300 cm³ s⁻¹ (tidal volume=750 cm³ and inhalation time=2.5 s) and different puff and breath-hold scenarios (see caption of Fig. 8). For comparison, mass deposition without considering coagulation for normal bolus inhalation and for normal physiological breathing are also plotted.

time of 2 s and breath-hold time of 1 s (Ingebrethsen et al., 2011). For comparison, differential number deposition without considering coagulation for bolus inhalation (0_0, noC) and for normal physiological breathing (NPB, noC), i.e. over the whole inspiratory phase, are also plotted.

Comparison of normal bolus inhalation considering coagulation with bolus inhalation without considering coagulation illustrates the effect of coagulation by increasing particle diameters and thus slightly reducing deposition by Brownian motion. Since particles inhaled at the beginning of the inhalation phase penetrate deeper into the lungs as compared to the

same number of particles uniformly inspired over the whole inhalation period (normal physiological breathing), bolus inhalation without breath-hold increases particle deposition relative to normal physiological breathing. With increasing breath-hold time, however, coagulation in the mouth not only decreases the number of particles entering the lung, but also increases particle diameters and hence reduces deposition by diffusion (see Fig. 7).

Corresponding differential mass deposition, assuming a density of 1.12 g cm^{-3} (Lipowicz, 1988) is displayed in Fig. 10, exhibiting the same tendencies as for the number distribution (Fig. 9). Bolus deposition is again higher than for normal breathing, and increasing breath-hold times lead to lower mass deposition, although to a lesser extent than for number deposition, because larger particles experiencing stronger gravitational forces carry a higher mass. By the same token, the difference between normal bolus inhalation considering coagulation with bolus inhalation without considering coagulation is significantly greater for mass deposition.

The relationship between differential mass deposition and related particle diameters is plotted in Fig. 11 for the same breathing scenarios discussed in Figs. 9 and 10, further supporting the above discussion on the effect of coagulation on particle diameters and the role of breath-hold times.

Numerical values for the related number and mass depositions and count and mass median diameters for all breathing scenarios exhibited in Figs. 9 and 10 are listed in Tables 1 and 2.

Inhaled (entering the lung and the mouth, respectively) and exhaled (exiting the mouth) number distributions of inhaled 150 nm CMD particles (GSD=1.44) for a flow rate of 300 cm^3 s^{-1} for the standard puff and breath-hold scenario are plotted
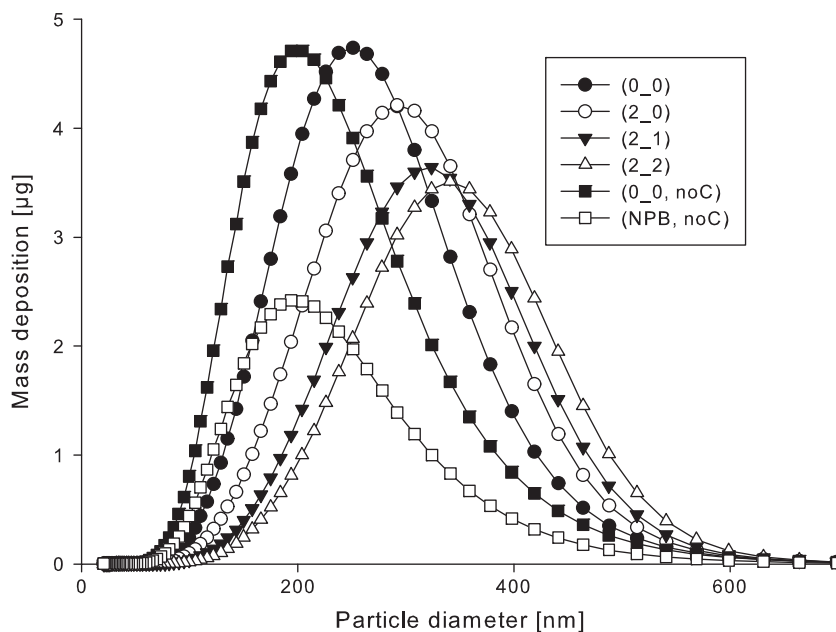
Fig. 11. Mass deposition of inhaled 150 nm CMD particles (GSD=1.44) (inhaled particle concentration=1.54 × 10^9 particles per cm^3) for a flow rate of 300 cm^3 s^{-1} (tidal volume=750 cm^3 and inhalation time=2.5 s) and different puff and breath-hold scenarios (see caption of Fig. 8). For comparison, mass deposition without considering coagulation for normal bolus inhalation and for normal physiological breathing are also plotted.
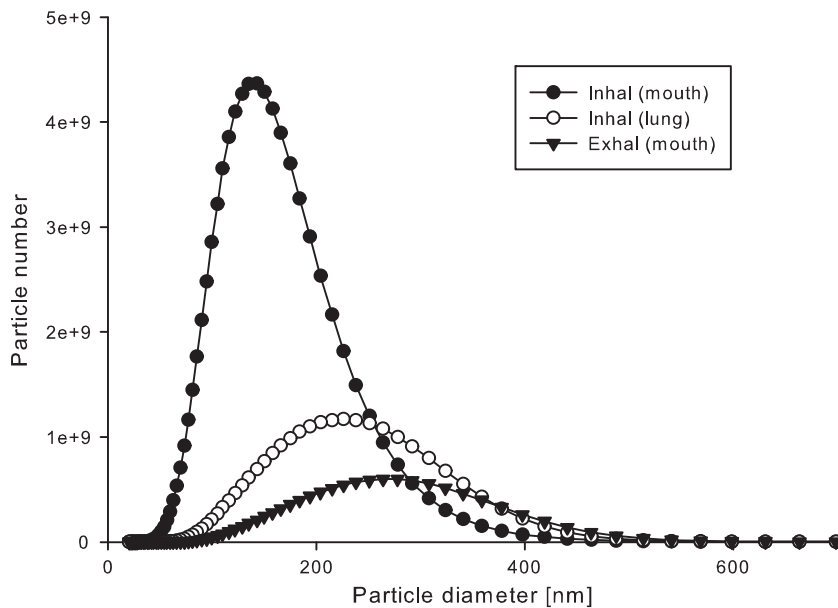
Table 1
Total number and mass deposition fractions of inhaled 150 nm CMD particles (GSD=1.44) (inhaled particle concentration=1.54 × 10^9 particles per cm^3) in the human respiratory tract for a flow rate of 300 cm^3 s^{-1} (tidal volume=750 cm^3 and inhalation time=2.5 s) and different puff and breath-hold scenarios: (0_0) normal bolus breathing (0_0), puff time=2 s, no breath-hold (2_0), puff time=2 s, breath-hold time=1 s (2_1), and puff time=2 s, breath-hold time=2 s (2_2). For comparison, number and mass deposition fractions without considering coagulation (0_0, noC) are also listed.

Inhalation scenarios					
Deposition parameters	(0_0)	(2_0)	(2_1)	(2_2)	(0_0, noC)
Number deposition fraction (%)					
ET	16.5	53.83	71.92	79.2	1.52
Lung	62.02	28.89	14.51	9.61	44.25
Mass deposition fraction (%)					
ET	1.2	7.08	16.56	20.54	1.65
Lung	32.06	26.55	21.02	19.35	38.07

Table 2

Count median (CMD) and mass median (MMD) diameters and related geometric standard deviations (GSD) of inhaled 150 nm CMD particles with a GSD of 1.44 when entering the trachea (lung) and exiting the mouth lung for a flow rate of 300 cm³ s⁻¹ (tidal volume=750 cm³ and inhalation time=2.5 s) and different puff and breath-hold scenarios (see Table 1). For comparison, inhaled and exhaled size distributions without considering coagulation are also listed.

| Inhalation scenarios					
Deposition parameters	(0_0)	(2_0)	(2_1)	(2_2)	(0_0, noC)
CMD [nm]					
Inhalation (trachea)	149	177	205	225	140
(GSD)	(1.44)	(1.46)	(1.44)	(1.43)	(1.45)
Exhalation (mouth)	208	223	240	255	146
(GSD)	(1.44)	(1.45)	(1.43)	(1.42)	(1.43)
MMD [nm]					
Inhalation (trachea)	221	272	307	332	209
(GSD)	(1.35)	(1.3)	(1.28)	(1.28)	(1.36)
Exhalation (mouth)	310	336	352	368	213
(GSD)	(1.28)	(1.28)	(1.27)	(1.26)	(1.38)

Fig. 12. Inhaled (entering the mouth and the lung, respectively) and exhaled (exiting the mouth) number distributions of inhaled 150 nm CMD particles (GSD=1.44) for a flow rate of 300 cm³ s⁻¹ (tidal volume=750 cm³ and inhalation time=2.5 s) for the standard puff and breath-hold scenario (2_1) (see caption of Fig. 8) (inhaled particle concentration=1.54×10^9 particles per cm³).

in Fig. 12. This figure clearly demonstrates the primary reduction of inhaled particles in the respiratory tract that occur in the mouth due to coagulation, accompanied by a significant shift of the size distribution to larger particle diameters. In the lung, particle loss is caused primarily by deposition due to diffusion with a preferential deposition for smaller particle diameters.

Corresponding differential mass distributions for the standard puff and breath-hold scenario are displayed in Fig. 13. Again a shift to larger particle diameters can be observed, but the reduction of the total mass after one breath is much smaller as compared to the number distribution shown in Fig. 12.

In the case of normal physiological inhalation at sufficiently low particle concentrations, say below 10^6 particles per cm³, the number distribution of deposited particles can be obtained experimentally by subtracting the number of exhaled from the number of inhaled particles in each size bin. For high inhaled particle concentrations, however, as in the case of inhaled cigarette smoke particles, where coagulation plays a dominant role, this leads to negative values in the size range from about 250 to 500 nm (Fig. 14). This apparent deficit indicates that the production of particles in this size range by coagulation of smaller-sized particles is greater than the loss from coagulation to larger sizes and deposition. Since this deficit is less significant for deposition in the lung, this suggests (i) that coagulation processes dominate particle loss in the mouth and (ii) that particle loss in the lung is caused not only by coagulation but also by physical deposition mechanisms.
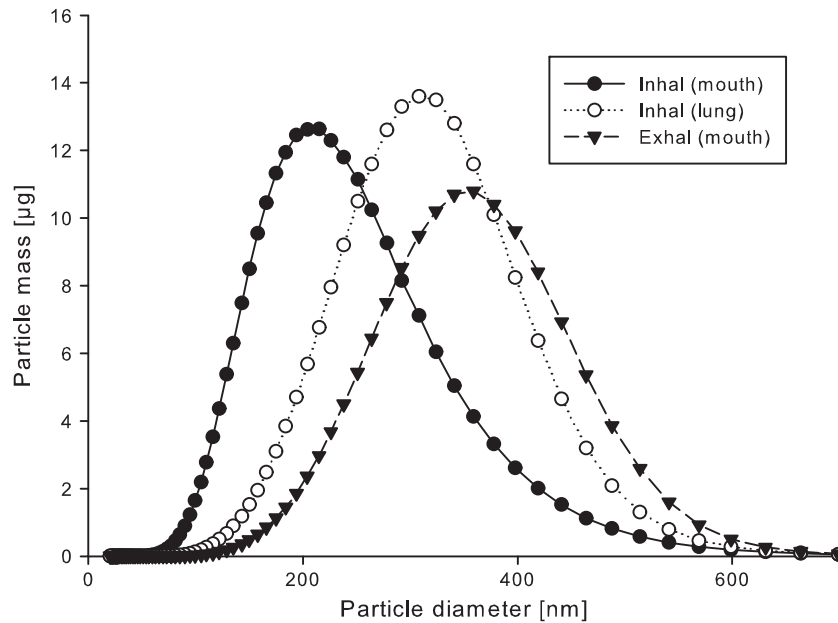
Fig. 13. Inhaled (entering the mouth and the lung, respectively) and exhaled (exiting the mouth) mass distributions of inhaled 150 nm CMD particles (GSD=1.44) for a flow rate of 300 cm^3 s^{-1} (tidal volume=750 cm^3 and inhalation time=2.5 s) for standard puff and breath-hold scenario (2_1) (see caption of Fig. 8) (inhaled particle concentration=1.54 × 10^9 particles per cm^3).
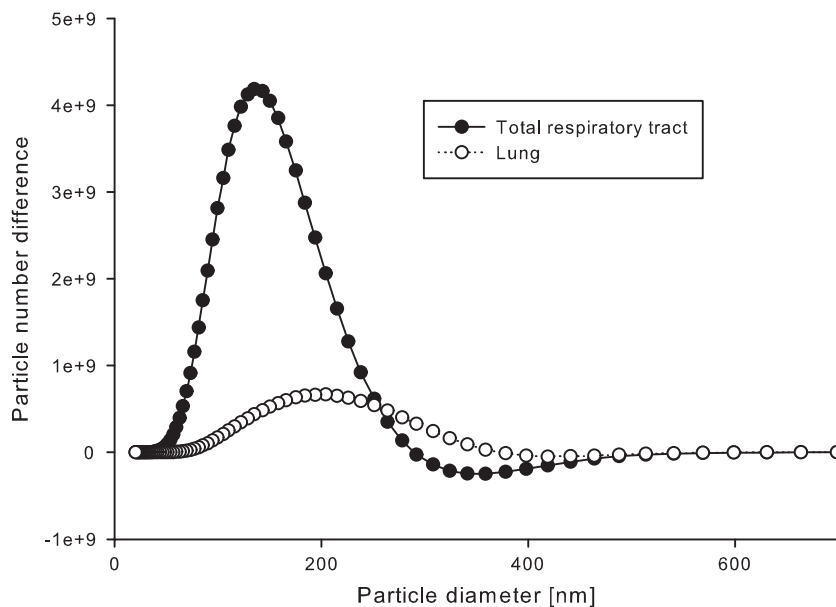
Fig. 14. Difference between inhaled and exhaled number distributions in the total respiratory tract (i.e., from mouth to mouth) and for the lung (i.e. from trachea to trachea) for inhaled 150 nm CMD particles (GSD=1.44) (inhaled particle concentration=1.54 × 10^9 particles per cm^3) for a flow rate of 300 cm^3 s^{-1} (tidal volume=750 cm^3 and inhalation time=2.5 s) for the standard puff and breath-hold scenario (2_1) (see caption of Fig. 8).

4. Discussion and conclusion

To validate the present coagulation and deposition calculations, theoretical predictions were compared with unpublished experimental data on total and oral (i.e., mouth-only inhalation) deposition supplied by BAT (British American Tobacco). Note that measured and computed deposition fractions are defined as the loss of particles both by coagulation and by physical particle deposition mechanisms in the mouth and the lung. Deposition or loss fractions were obtained by subtracting the exhaled total particle number from the corresponding inhaled particle number. The experimental data sets, each obtained from one volunteer, provide information on six consecutive puffs with an average puff time of 2.5 s and an

average puff volume of 65 mL. As already observed by Alderman & Ingebrethsen (2011), the experimental data indicate that particle concentrations increased and particle diameters decreased with rising puff number.

Theoretical predictions of total and oral deposition (loss) fractions are compared with the available experimental data in Tables 3 and 4. Excellent agreement between predicted total and oral deposition (loss) fractions and the measured values can be observed, with deviations of only a few percent. Since number deposition (loss) is dominated by particle loss due to coagulation, this suggests that the coagulation model works properly in both the oral and thoracic region.

In the present study, the impact of coagulation of cigarette smoke aerosols on deposition in the human lung was simulated for varying smoking patterns and typical inhalation and exhalation conditions. The coagulation sources considered include thermal diffusion of charged and uncharged particles, gravitational settling, particles' differences in inertia, and laminar shear and turbulences of the flow, respectively.

The relative change in particle number concentration due to coagulation was estimated using the approximation as described in Section 2 for thermal, laminar shear and turbulent coagulation, respectively, for a particle diameter of 150 nm and a concentration of 1.54×10^9 particles per cm^3. The resulting changes were > 1 for thermal coagulation and of the order of 10^{-3} and 10^{-4} in the cases of laminar shear and turbulent coagulation. Numerical simulations of coagulation mechanisms, as described in Section 2.1, gave a relative change in particle number concentration of roughly 85% for thermal, 7% for laminar shear, 0.4% for settling, 0.3% for turbulent and $\ll 1\%$ for coagulation at bifurcations. The influence of charge on thermal coagulation had only a negligible effect for the charge distribution considered (Robinson & Yu, 1999). Note that the numbers calculated were derived for 2 s puff time, 1 s breath-hold time, no dilution and in absence of deposition.

For similar breathing conditions and a charge distribution as applied throughout this work, thermal diffusion is by far the biggest contributor to coagulation. Laminar shear coagulation and turbulent coagulation may increase their contribution for different breathing conditions, while the effects of settling coagulation and coagulation at bifurcations are relatively limited, since an increasing relative velocity of two particles shortens the time for coagulation.

Coagulation reshapes the inhaled particle size distribution by shifting it to higher particle diameters and simultaneously decreasing the total number deposition. Hence experimental determination of deposited particle fractions is a bit misleading, since number deposition comprises the loss of inhaled particles not only by deposition but also by coagulation. In contrast, experimental determination of total deposited mass is not directly affected by coagulation. Although coagulation can simply be avoided by diluting the aerosol, dilution of partly volatile aerosols that interact with the surrounding vapor phase is accompanied by a loss in information on particle composition and size.

Reduction of particle mass in the mouth by deposition was calculated considering gravitational settling, diffusion and impaction. Depending on the puffing and breath-hold times, mass deposition fractions range from 1% (normal physiological

Table 3
Comparison between measured and predicted total number deposition (loss) fractions (DF) for inhaled cigarette smoke. *Note*: "Deposition" fractions comprise loss of particles by coagulation and by physical particle deposition mechanisms.

| Puff | CMD* | Concentration | DF (%) | | Ratio IDEAL/EXP |
	(nm)	($^*10^9$ cm^{-3})	EXP	IDEAL	
Puff 1	216	1.61	78.9	79.6	1
Puff 2	210	1.43	74.8	78.7	1.05
Puff 3	203	2.73	83.8	86.6	1.03
Puff 4	207	3.34	86.6	89.1	1.03
Puff 5	195	3.6	88.1	88.7	1
Puff 6	185	4.32	88.6	91.2	1.03

* GSD=1.46.

Table 4
Comparison between measured and predicted oral number deposition (loss) fractions (DF) in case of no inhalation. *Note*: "Deposition" fractions comprise loss of particles by coagulation and by physical particle deposition mechanisms.

| Puff | CMD* | Concentration | DF (%) | | Ratio IDEAL/EXP |
	(nm)	($^*10^9$ cm^{-3})	EXP	IDEAL	
Puff 1	189	2.23	81	80	0.99
Puff 2	195	1.99	75	76	1.01
Puff 3	211	1.92	73	76	1.04
Puff 4	195	2.63	76	83	1.09
Puff 5	198	3.67	84	87	1.04
Puff 6	193	3.62	83	87	1.05

* GSD=1.46.

breathing) to 28% (2 s puff, 3 s breath-hold). For the standard smoking conditions (2 s puff, 1 s breath-hold), 16% of the inhaled mass are deposited in the oral region. For the submicron sizes of the inhaled cigarette smoke particles, diffusion is practically the only contributor to deposition.

Coagulation processes dominate particle loss in the mouth, with only a minor contribution by deposition mechanisms. In contrast, particle loss in the lung is caused by coagulation and deposition mechanisms. Within the puffing phase the particle concentration in the oral cavity is reduced by roughly 50%. The remaining particles are then again reduced by roughly 50% during the 1 s breath hold period, resulting in a 75% decrease in particle concentration in the oral cavity while the mass concentration remains constant.

For the particle size distributions observed throughout this work, coagulation reduces particle deposition in the lungs in terms of number, surface and mass. The particle size distribution initially inhaled contains a considerable fraction of small, fast diffusing particles that are practically removed due to coagulation. The size distribution thus shifts towards larger particles for which the lung represents a less efficient filter than for the initial size distribution.

In the present study, deposition patterns of inhaled highly concentrated particles in the mouth and in individual airway generations were computed to evaluate the effect of coagulation on local particle deposition. However, in the upper bronchial airways, where the effect of coagulation on particle deposition is most significant, two mechanisms may modify the predicted deposition patterns throughout the bronchial tree: cloud motion and mucociliary clearance.

Cloud motion or colligative effects are commonly discussed in context with cigarette smoke deposition (Martonen, 1992; Phalen et al., 1994; Hinds, 1999; Martonen & Musante, 2000; Robinson & Yu, 2001; Broday & Robinson, 2003; Zhang et al., 2012). Cloud motion occurs when an array of particles behaves as an entity that masks the behavior of its individual constituent particles (Martonen, 1992). Broday & Robinson (2003) provided a comprehensive mathematical formulation of the effect of cloud motion on diffusion, impaction and sedimentation in the human lung. Since the mouth is homogeneously filled with smoke particles upon inhalation, no cloud effects are expected to occur in the extrathoracic region. However, when the inhaled smoke column passes through the narrow glottis of the larynx, the resulting laryngeal jet (Chan et al., 1978) may form a cloud. Variables determining subsequent deposition of the cloud are the diameter of the cloud in the trachea and in downstream bronchial airways, relative to airway diameters, and the lifetime of the cloud when passing through the bronchial tree (Robinson & Yu, 2001; Broday & Robinson, 2003; Zhang et al., 2012). To analyze the effect of cloud motion on particle deposition, the equations supplied by Broday & Robinson (2003) were applied to the aerosol parameters and breathing patterns used in the present study. Variations of the cloud diameters and the lifetime of the cloud produced a wide range of deposition fractions. In general, cloud motion moves the deposition patterns for individual particles towards the large bronchial airways. Since no experimental data is currently available to justify the selection of any value of the cloud diameters in the airways and the lifetime of the cloud, no definitive answer of the role of cloud motion can be given at present, although an effect of cloud motion may indeed exist on theoretical grounds.

Initial deposition patterns in human airways are readily modified by the action of several particle clearance mechanisms. The dominating clearance mechanism in bronchial airway is mucociliary motion, propelling the deposited particles towards the trachea (ICRP, 1994). While mucociliary action reduces the number of deposited particles in the upper bronchial airways, this removal is partly compensated by particles initially deposited in the peripheral parts of the lung and moved up to the bronchial airways by the mucociliary escalator (Hofmann & Sturm, 2004). As a consequence of this mucus transport, the number of particles in the lungs will continuously drop until all particles have left the lung (Hofmann & Asgharian, 2003).

In conclusion, the excellent agreement between calculated total and oral number deposition (loss) and the available experimental evidence indicates that the present coagulation model correctly predicts particle number losses. It therefore adds some confidence in the validity of our predictions of the related mass deposition fractions.

Acknowledgments

Appendix A

This section presents the derivation of the coagulation rate due to collisions of particles at airway bifurcations caused by particle inertia. Let us assume that particles travel with speed v_d, being equal to the air flow velocity v_{gas}, along the streamlines. At a bifurcation with branching angle Θ (i.e. the angle formed by the initial gas flow direction in the parent airway and the new gas flow direction in the daughter airway), particles may leave the streamlines with a speed component $v_{d,rel}$ perpendicular to the direction of the air flow. In first approximation this relative speed can be written as:

$$v_{d,rel} = v_{gas} \sin(\Theta) \tag{A1}$$

The time t particle i adopts the speed component perpendicular to the streamlines can be written as a function of stopping distance S and relative speed $v_{d,rel}$ (Hinds, 1999):

$$t_i = \frac{S_i}{v_{gas} \sin(\Theta)} \tag{A2}$$

To determine particle coagulation due to changes of air flow direction at a bifurcation, the formulation for the coagulation coefficient for gravitational settling is applied with a single change in the expression, i.e. the source of relative motion, which is the difference in settling velocity Δv, is replaced by a term that takes into account differences in relative motion due to deviation from the streamlines:

$$\Delta v = \frac{\Delta S}{\Delta t} = v_{gas} \sin(\Theta) \tag{A3}$$

with

$$\Delta S = |S_i - S_j| \tag{A4}$$

and

$$\Delta t = \left| \frac{S_i}{v_{d,i,rel}} - \frac{S_j}{v_{d,j,rel}} \right| = \frac{1}{v_{gas} \sin(\Theta)} |S_i - S_j| \tag{A5}$$

Thus the coagulation coefficient $\beta_{bif,ij}$ for particles impacting on each other caused by relative motions at bifurcations can be written as:

$$\beta_{bif,ij} = \pi \left(\frac{d_i + d_j}{2} \right)^2 v_{gas} \sin(\Theta) E_{ij} \tag{A6}$$

with E_{ij} being the empirical efficiency for particle i being captured by particle j. Note that all characteristic particle properties do not occur in the equation for the relative speed. However, they reenter the equation when coagulation is calculated by integration of the coagulation coefficient over time as the time for coagulation is represented by Δt (see Eq. (A5)).

Appendix B. Supporting information

Supplementary data associated with this article can be found in the online version at http://dx.doi.org/10.1016/j.jaerosci.2013.05.007.

References

Adam, T, McAughey, J, McGrath, C, Mocker, C, & Zimmermann, R (2009). Simultaneous online size and chemical analysis of gas phase and particulate phase of cigarette mainstream smoke. *Analytical and Bioanalytical Chemistry, 394*, 1193–1203.

Alderman, S.L., & Ingebrethsen, B.J. (2011). Characterization of mainstream cigarette smoke particle size distribution from commercial cigarettes using a DMS500 fast particulate spectrometer and smoking cycle simulator. *Aerosol Science and Technology, 45*, 1409–1421.

Balásházy, I., Hofmann, W., & Heistracher, T. (2003). Local particle deposition patterns may play a key role in the development of lung cancer. *Journal of Applied Physiology, 94*, 1719–1725.

Broday, D.M., & Robinson, R. (2003). Application of cloud dynamics to dosimetry of cigarette smoke particles in the lungs. *Aerosol Science and Technology, 37*, 510–527.

Cai, F.S., & Yu, C.P. (1988). Inertial and interceptional deposition of spherical particles and fibers in a bifurcating airway. *Journal of Aerosol Science, 19*, 679–688.

Chan, T.L., Lippmann, M, Cohen, V.R., & Schlesinger, R.B. (1978). Effect of electrostatic charges on particle deposition in a hollow cast of the human larynx-tracheobronchial tree. *Journal of Aerosol Science, 9*, 463–468.

Chan, T.L., Schreck, R.M., & Lippmann, M. (1980). Effect of the laryngeal jet on particle deposition in the human trachea and upper bronchial airways. *Journal of Aerosol Science, 11*, 447–459.

Cheng, Y.S. (2003). Aerosol deposition in the extrathoracic region. *Aerosol Science and Technology, 37*, 659–671.

Cohen, B.S., & Asgharian, B. (1990). Deposition of ultrafine particles in the upper airways: an empirical analysis. *Journal of Aerosol Science, 21*, 789–797.

Einstein, A. (1905). The motion of elements suspended in static liquids as claimed in the molecular kinetic theory of heat. *Annalen der Physik, 17*, 549–560.

Farkas, Á., Balásházy, I., & Szöcs, K. (2006). Characterization of regional and local deposition of inhaled drugs in the respiratory system by computational fluid and particles dynamics methods. *Journal of Aerosol Medicine, 19*, 329–343.

Ferron, G.A., Kreyling, W.G., & Haider, B. (1988). Inhalation of salt aerosol particles—II. Growth and deposition in the human respiratory tract. *Journal of Aerosol Science, 19*, 611–631.

Finlay, W.H. (2001). *The Mechanics of Inhaled Pharmaceutical Aerosols: An Introduction*. Academic Press: London.

Fuchs, N.A. (1964). *The Mechanics of Aerosols*. Pergamon Press: Oxford.

Haefeli-Bleuer, B., & Weibel, E.R. (1988). Morphometry of the human pulmonary acinus. *The Anatomical Record, 220*, 401–414.

Heyder, J., Gebhart, J., Rudolf, G., Schiller, C.F., & Stahlhofen, W. (1986). Deposition of particles in the human respiratory tract in the size range 0.005 to 15 μm. *Journal of Aerosol Science, 17*, 811–825.

Hinds, W.C. (1999). *Aerosol Technology: Properties, Behavior, and Measurement of Airborne Particles*. John Wiley & Sons: New York.

Hofmann, W. (2011). Modelling inhaled particle deposition in the human lung—A review. *Journal of Aerosol Science, 42*, 693–724.

Hofmann, W., & Asgharian, B. (2003). The effect of lung structure on mucociliary clearance and particle retention in human and rat lungs. *Toxicological Science, 73*, 448–456.

Hofmann, W., & Koblinger, L. (1990). Monte Carlo modeling of aerosol deposition in human lungs. Part II: Deposition fractions and their sensitivity to parameter variations. *Journal of Aerosol Science, 21*, 674–688.

Hofmann, W., & Sturm, R. (2004). Stochastic model of particle clearance in human bronchial airways. *Journal of Aerosol Medicine, 17*, 73–89.

Hofmann, W., Asgharian, B., & Winkler-Heil, R. (2002). Modeling intersubject variability of particle deposition in human lungs. *Journal of Aerosol Science, 33*, 219–235.

Hofmann, W., Pawlak, E., & Sturm, R. (2008). Semi-empirical stochastic model of aerosol bolus dispersion in the human lung. *Inhalation Toxicology, 20*, 1059–1073.

Ingham, D.B. (1975). Diffusion of aerosols from a stream flowing through a cylindrical tube. *Journal of Aerosol Science, 6*, 125–132.

International Commission on Radiological Protection (ICRP) 1994. Human respiratory tract model for radiological protection. ICRP Publication 66. *Annals of the ICRP*, 24, Nos 1–3.

Ingebrethsen, B.J., Alderman, S.L., & Ademe, B. (2011). Coagulation of mainstream cigarette smoke in the mouth during puffing and inhalation. *Aerosol Science and Technology*, 45, 1422–1428.

Kane, D.B., Asgharian, B., Price, O.T., Rostami, A., & Oldham, M.J. (2010). Effect of Smoking Parameters on the Particle Size Distribution and Predicted Airway Deposition of Mainstream Cigarette Smoke. *Inhalation Toxicology*, 22, 199–209.

Koblinger, L., & Hofmann, W. (1990). Monte Carlo modeling of aerosol deposition in human lungs. Part I: simulation of particle transport in a stochastic lung structure. *Journal of Aerosol Science*, 21, 661–674.

Koblinger, L., & Hofmann, W. (1985). Analysis of human lung morphometric data for stochastic aerosol deposition calculations. *Physics in Medicine and Biology*, 30, 541–556.

Lipowicz, P.J. (1988). Determination of cigarette smoke particle density from mass and mobility measurements in a Millikan cell. *Journal of Aerosol Science*, 19, 587–589.

Longest, P.W., & Kleinstreuer, C. (2005). Computational models for simulating multicomponent aerosol evaporation in the upper respiratory airways. *Aerosol Science and Technology*, 39, 124–138.

Martonen, T.B. (1992). Deposition patterns of cigarette smoke in human airways. *American Industrial Hygiene Association Journal*, 53, 6–16.

Martonen, T.B. (1993). A mathematical model for the selective deposition of inhaled pharmaceuticals. *Journal of Pharmaceutical Sciences*, 82, 1191–1199.

Martonen, T.B., & Musante, C.J. (2000). Importance of cloud motion on cigarette smoke deposition in lung airways. *Inhalation Toxicology*, 12, 261–280.

Mitsakou, C., Helmis, C., & Housiadas, C. (2004). Eulerian modelling of lung deposition with sectional representations of aerosol dynamics. *Journal of Aerosol Science*, 36, 75–94.

Phalen, R.F., Oldham, M.J., & Mannix, R.C. (1994). Cigarette smoke deposition in the tracheobrocnhial tree: evidence for colligative effects. *Aerosol Science and Technology*, 20, 215–226.

Raabe, O. G., Yeh, H. C., Schum, G. M. & Phalen, R. F., Tracheobronchial geometry: human, dog, rat, hamster, 1976, Lovelace Foundation Report LF-53; Lovelace Foundation.

Robinson, R., & Yu, C.P. (1998). Theoretical analysis of hygroscopic growth rate of mainstream and sidestream cigarette smoke particles in the human respiratory tract. *Aerosol Science and Technology*, 28, 21–32.

Robinson, R., & Yu, C.P. (1999). Coagulation of cigarette smoke particles. *Journal of Aerosol Science*, 30, 533–548.

Robinson, R., & Yu, C.P. (2001). Deposition of cigarette smoke particles in the human respiratory tract. *Aerosol Science and Technology*, 34, 202–215.

Saffmann, P., & Turner, J. (1956). On the collisions of drops in turbulent clouds. *Journal of Fluid Dynamics*, 1, 16–30.

Schiller, C.F., Gebhart, J., Heyder, J., Rudolf, G., & Stahlhofen, W. (1988). Deposition of monodisperse insoluble aerosol particles in the 0.005 to 0.2 μm size range within the human respiratory tract. *Annals of Occupational Hygiene, Suppl*, 1, 41–49.

Smoluchowski, M.V. (1917). Versuch einer mathematischen Theorie der Koagulationskinetik kolloider Lösungen. *Zeitschrift für Physikalische Chemie*, 92, 129–168.

Stahlhofen, W., Rudolf, G., & James, A.C. (1989). Intercomparison of experimental regional aerosol deposition data. *Journal of Aerosol Medicine*, 2, 285–308.

Truesdell, C., & Muncaster, R.G. (1980). *Fundamentals of Maxwell's Kinetic Theory of a Simple Monatomic Gas*. Academic Press: New York.

Zebel, G. (1966). Coagulation of Aerosols. In C.N. Davies (Ed.), *Aerosol Science*. Academic Press: New York, pp. 31–58.

Zhang, Z., Kleinstreuer, C., & Hyun, S. (2012). Size-change and deposition of conventional and composite cigarette smoke particles during inhalation in a subject-specific airway model. *Journal of Aerosol Science*, 46, 34–52.

Zhang, Z., Kleinstreuer, C., & Kim, C.S. (2009). Comparison of analytical and CFD models with regard to micron particle deposition in a human 16-generation tracheobronchial airway model. *Journal of Aerosol Science*, 40, 16–28.